Supporting Information

Theoretical Mechanistic Study of Novel Ni(0)-Catalyzed [6−2+2] Cycloaddition Reactions of Isatoic Anhydrides with Alkynes: Origin of Facile Decarboxylation

Wei Guan,[†] Shigeyoshi Sakaki[*,†] Takuya Kurahashi,[‡] and Seijiro Matsubara,[‡]

[†]Fukui Institute for Fundamental Chemistry, Kyoto University, Kyoto 606-8103, Japan

[‡]Department of Material Chemistry, Graduate School of Engineering, Kyoto University, Kyoto 615-8510, Japan

1. Evaluation of Computational Methods

Two types of interactions play important roles in the present reaction. They are the steric repulsion between ligands and the electronic interaction between the Ni center and ligands. So, the performances of computational methods depend on the description of two types of interactions. First, in order to separately evaluate the steric repulsion between ligands, the model reaction was constructed without considering nickel, as shown in Scheme S1. **1a-without Ni** and **1a^{AL1}-without Ni** are derived from **1a** and **1a^{AL1}** optimized by B3PW91[S1] hybrid functional together with BS-I basis set. Then the steric repulsion evaluation (single point calculation) was carried out using ten different methods, spin component-scaled MP2 (SCS-MP2),[S2] MP2,[S3] M06,[11] M06L,[S4] M062X,[S5] B3PW91,[S1] PBE0,[S6] B97D,[S7] ωB97XD,[S8] and TPSSTPSS[S9] with 6-311+G(2d,p) basis set,[S10] as shown in Table S1. Compared with the SCS-MP2 result, testing has shown that B97D is the best; M06 and M06L are second choice. Obviously, B3PW91 overestimates the intramolecular steric repulsion.

Scheme S1. Model reaction to evaluate the steric repulsion between ligands

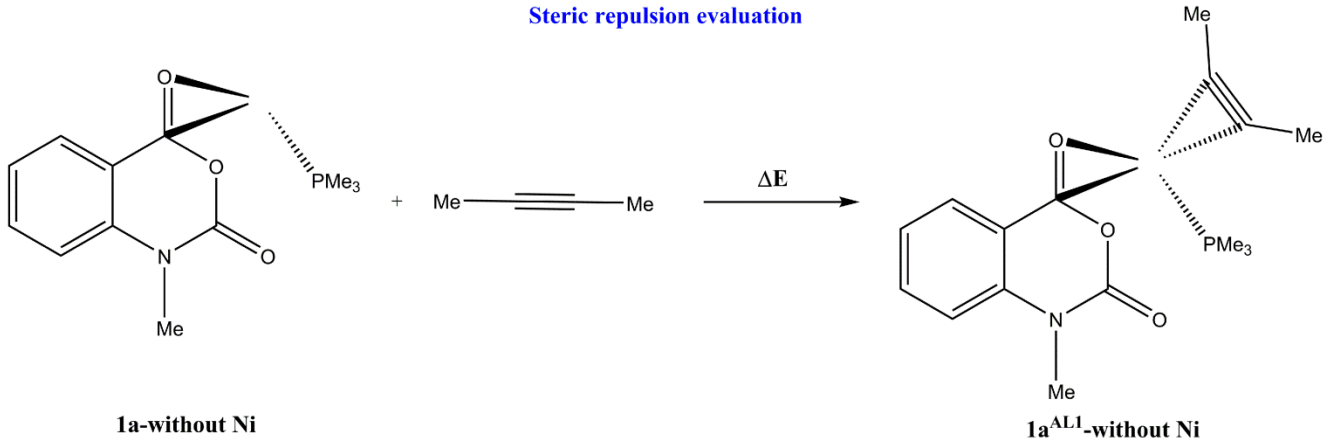

Table S1. Reaction energies of model reaction shown in Scheme S1 with various methods

	SCS-MP2	MP2	M06	M06L	M062X
ΔE (kcal/mol)	4.61	2.22	5.88	5.93	6.63
	B3PW91	PBE0	B97D	ωB97XD	TPSSTPSS
ΔE (kcal/mol)	14.29	11.39	4.95	6.68	11.60

*basis set: 6-311+G(2d,p) for H, P, C, N, and O.

Second, in order to evaluate the electronic interaction between the Ni center and ligands, a simple model reaction was proposed, as shown in Scheme S2. All geometries were optimized by B3PW91[S1] hybrid functional together with BS-I basis set. Then the electronic interaction evaluation (single point calculation) was performed using fifteen different methods, CCSD(T),[S11] CCSD,[S11] MP4(SDQ),[S12] MP4(DQ),[S12] MP4(D),[S12] MP3,[S13] MP2,[S3] M06,[11] M06L,[S4] M062X,[S5] B3PW91,[S1] PBE0,[S6] B97D,[S7] ωB97XD,[S8] and TPSSTPSS[S9] with BS-II basis set,[S10] as shown in Table S2. Compared with the CCSD(T) result, M06L is the best, whereas M06 becomes second choice. In addition, B3PW91 underestimates the interaction between alkyne and Ni moiety.

Scheme S2. Model reaction to evaluate the electronic interaction between Ni and ligands

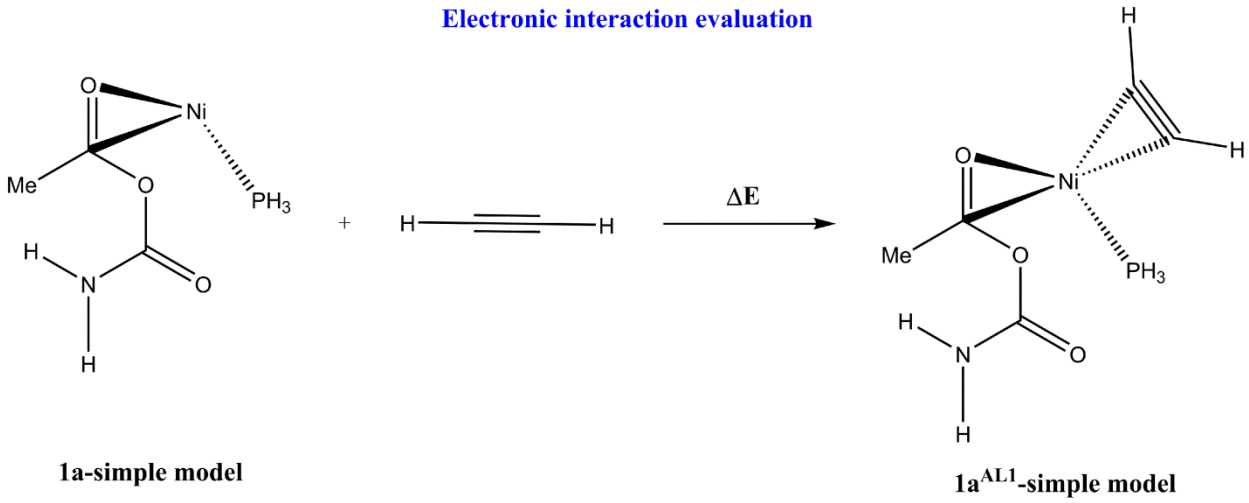

Table S2. Reaction energies of model reaction shown in Scheme S2 with various methods

	CCSD(T)	CCSD	MP4(SDQ)	MP4(DQ)	MP4(D)
ΔE (kcal/mol)	–18.45	–14.13	–18.83	–10.84	–10.93
	MP3	MP2	M06	M06L	M062X
ΔE (kcal/mol)	–9.25	–13.70	–16.54	–18.68	–12.47
	B3PW91	PBE0	B97D	ωB97XD	TPSSTPSS
ΔE (kcal/mol)	–13.08	–15.06	–13.84	–15.24	–16.38

*basis set: (311111/22111/411/11) for Ni and 6-311+G(2d,p) for H, P, C, N, and O.

In summary, considering the above two factors, hybrid functional M06 was selected to calculate all intermediates and transition states.

2. Correction of Translational Entropy in Solution

We provide energy (E_{sol}) with zero-point energy correction as well as the Gibbs energy (G^o_{sol}) in solution to discuss the reaction profile. For each species, the E_{sol} is defined through eqn (S1):

$$E_{sol} = E^{pot}_{sol} + E_{nonelect} + E^{v_0}_{gas} \tag{S1}$$

where $E^{v_0}_{gas}$ represents the zero-point vibrational energy in the gas phase. In a bimolecular process, such as the coordination of the substrate alkyne with the Ni(0), the entropy change must be taken into consideration because the entropy considerably decreases in the process. In this case, Gibbs energy (G^o_{sol}) must be evaluated as follows:

$$\begin{aligned} G^o_{sol} &= H_0 - T(S^o_r + S^o_v + S^o_t) \\ &= E^T + P\Delta V - T(S^o_r + S^o_v + S^o_t) \\ &= E_{sol} + E_{therm} - T(S^o_r + S^o_v + S^o_t) \end{aligned} \tag{S2}$$

where ΔV is 0 in solution, E_{therm} is the thermal correction by translational, vibrational, and rotational movements, and S^o_r, S^o_v, and S^o_t are rotational, vibrational, and translational entropies, respectively. In general, the Thacker-Tetrode equation is used to evaluate translational entropy S^o_t. In solution, however, the usual Thacker-Tetrode equation cannot be directly applied to the evaluation of S^o_t, because S^o_t is suppressed very much in solution.[S14] In this context, we evaluated the translational entropy with the method by developed by Whitesides et. al.[16]

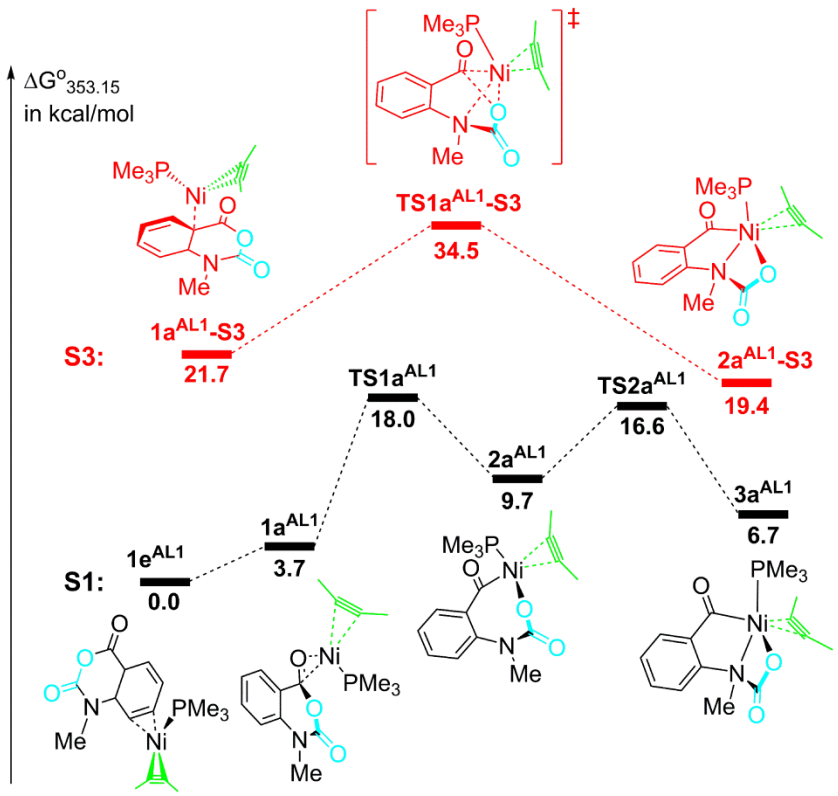

Figure S1. The singlet and triplet energy profiles ($\Delta G^{o}_{353.15}$) for the oxidative addition of isatoic anhydride to Ni(PMe_3)(but-2-yne).

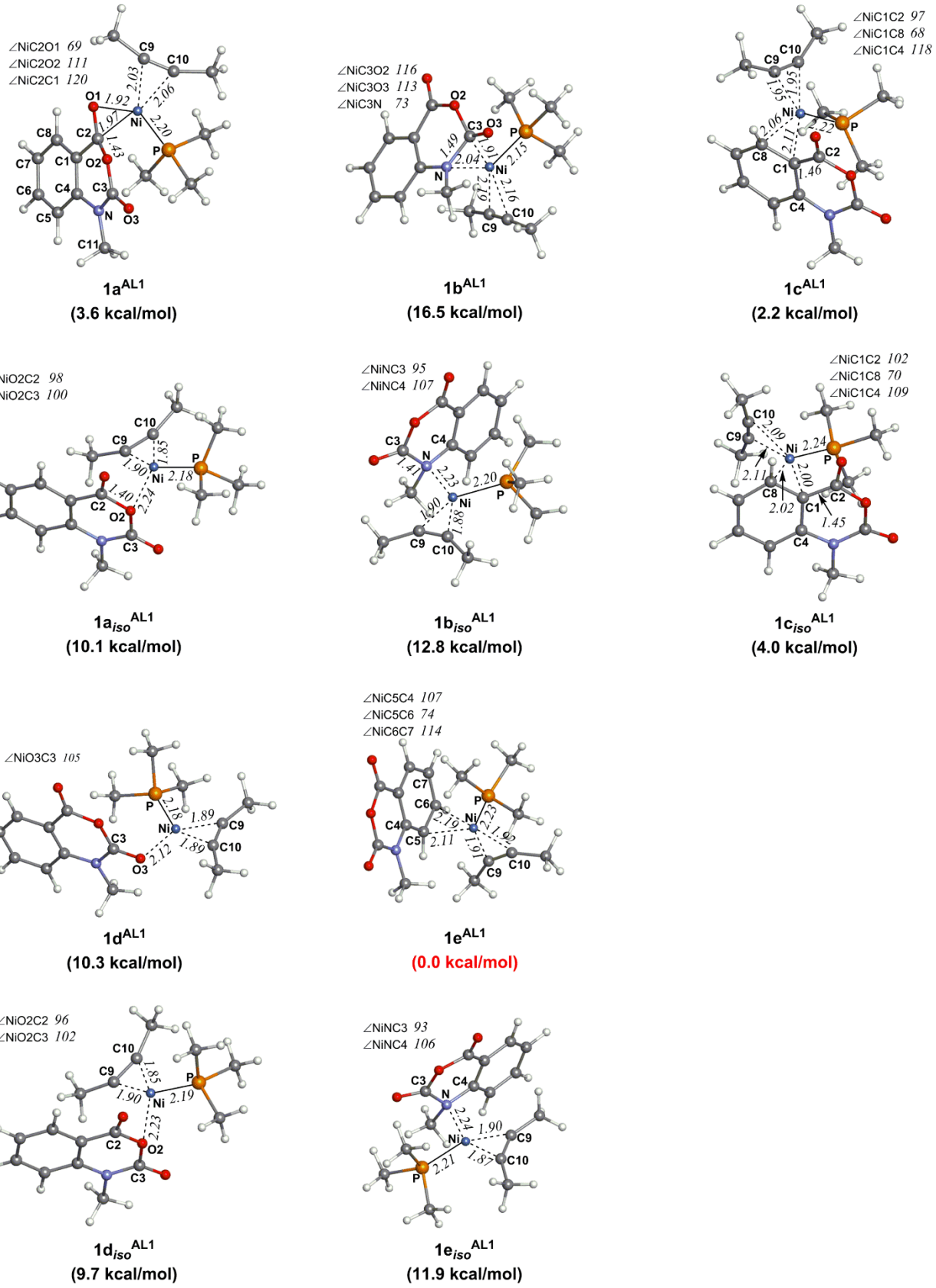

Figure S2. Optimized structures, selected geometrical parameters (bond length in angstrom unit and bond angle in degree) and relative energies (in kcal/mol) of ten complexes **1a**^{AL1}, **1a**$_{iso}$^{AL1}, **1b**^{AL1}, **1b**$_{iso}$^{AL1}, **1c**^{AL1}, **1c**$_{iso}$^{AL1}, **1d**^{AL1}, **1d**$_{iso}$^{AL1}, **1e**^{AL1}, and **1e**$_{iso}$^{AL1}.

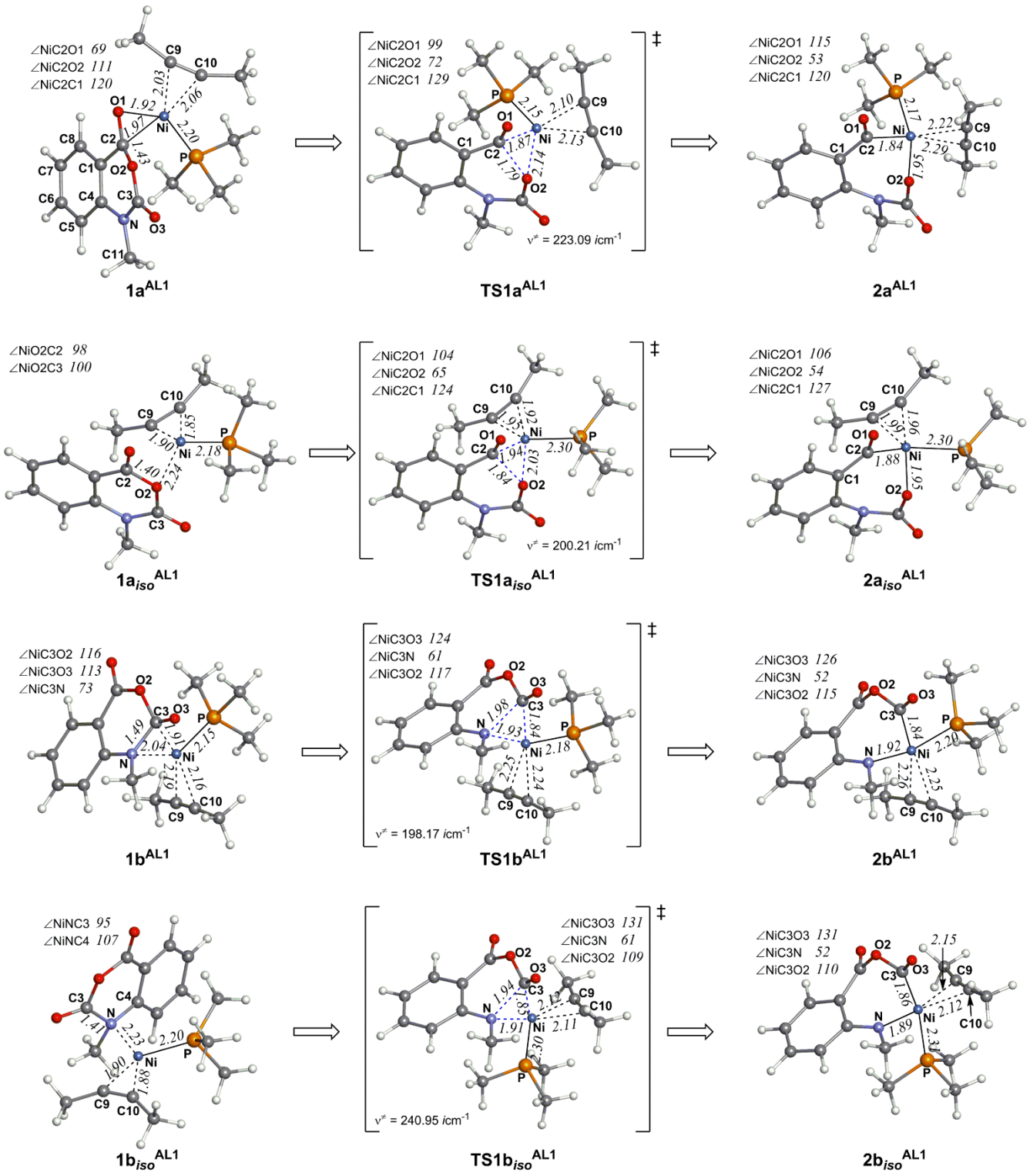

Figure S3-a. Optimized structures and selected geometrical parameters (bond length in angstrom unit and bond angle in degree) of stationary points in the oxidative addition of isatoic anhydride to Ni(PMe_3-)(but-2-yne).

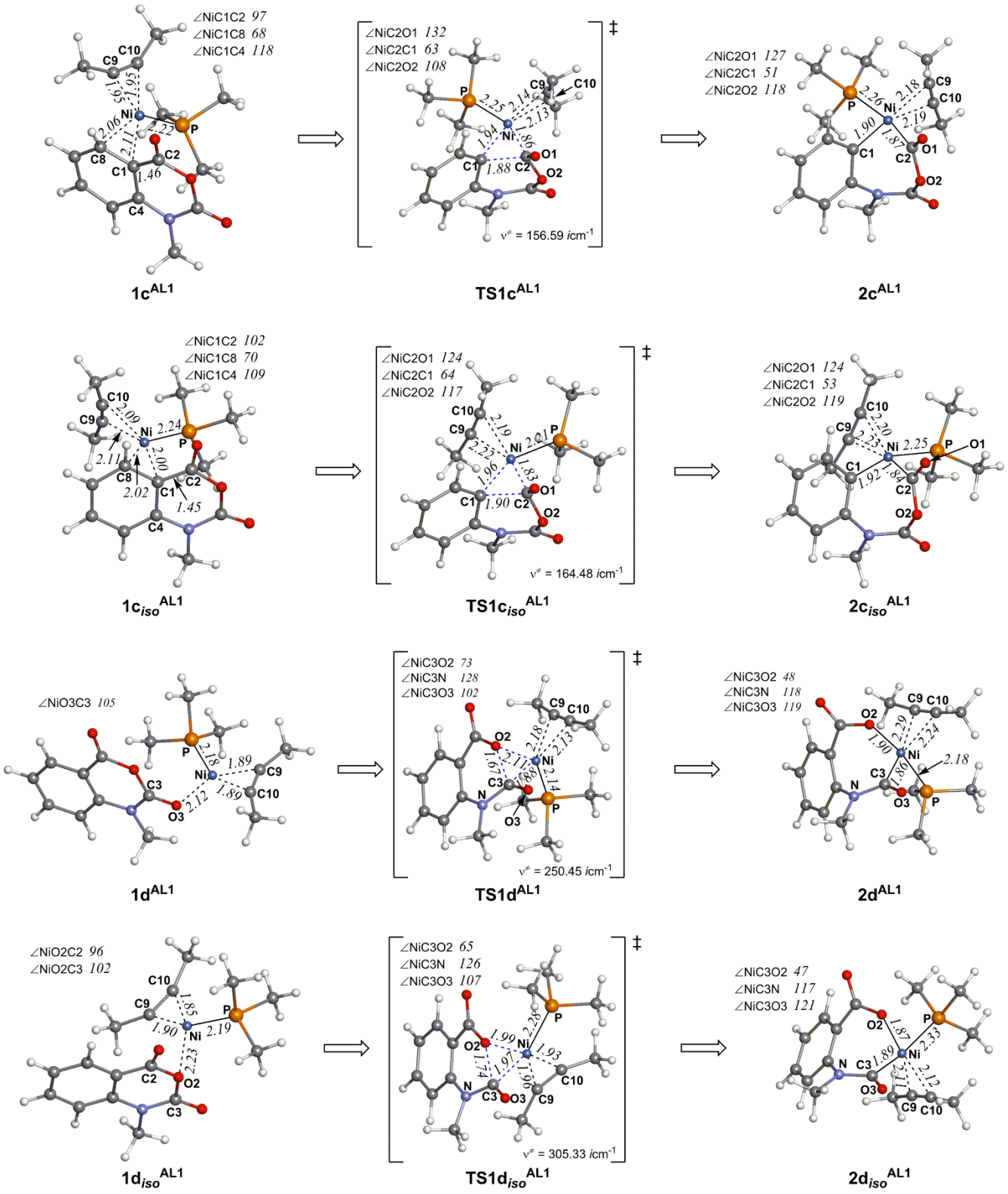

Figure S3-b. Optimized structures and selected geometrical parameters (bond length in angstrom unit and bond angle in degree) of stationary points in the oxidative addition of isatoic anhydride to Ni(PMe_3-)(but-2-yne).

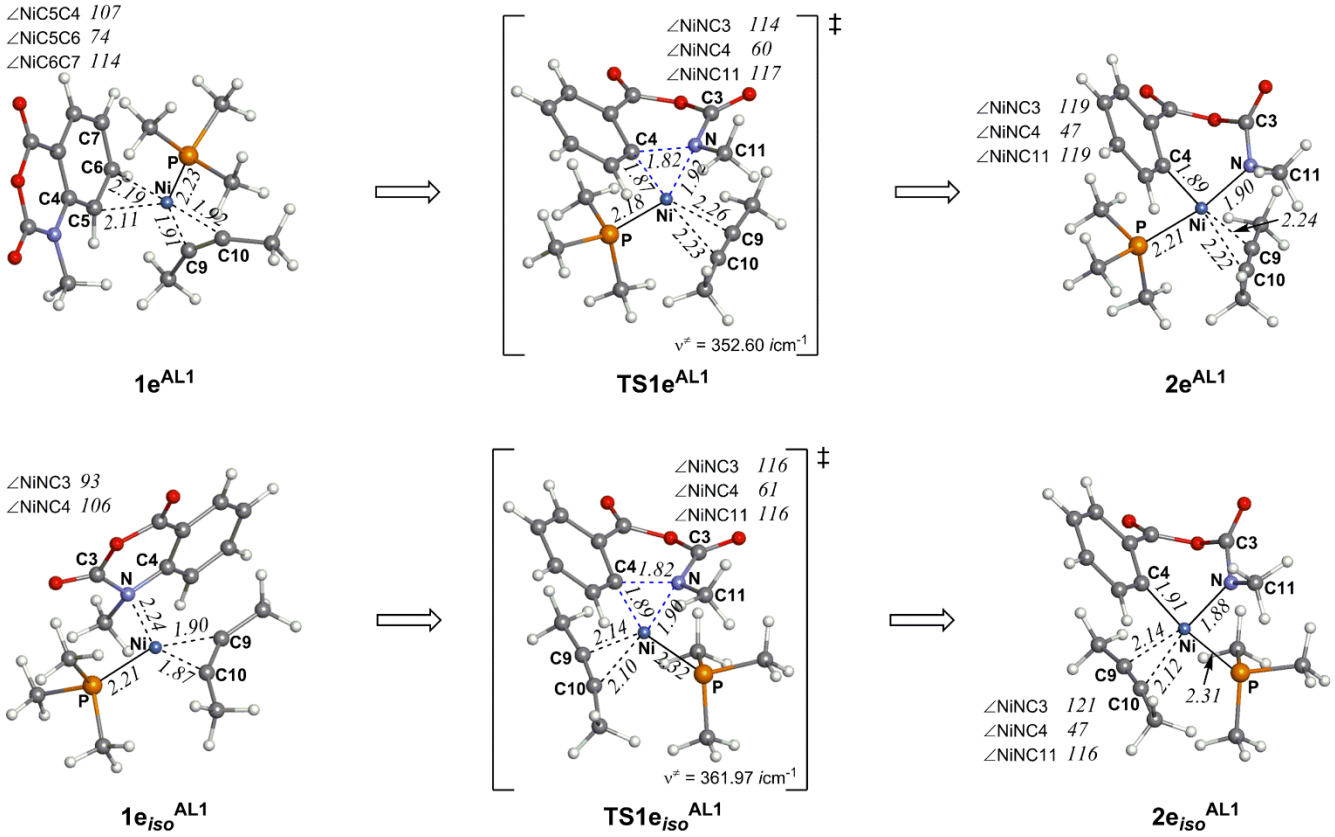

Figure S3-c. Optimized structures and selected geometrical parameters (bond length in angstrom unit and bond angle in degree) of stationary points in the oxidative addition of isatoic anhydride to Ni(PMe_3-)(but-2-yne).

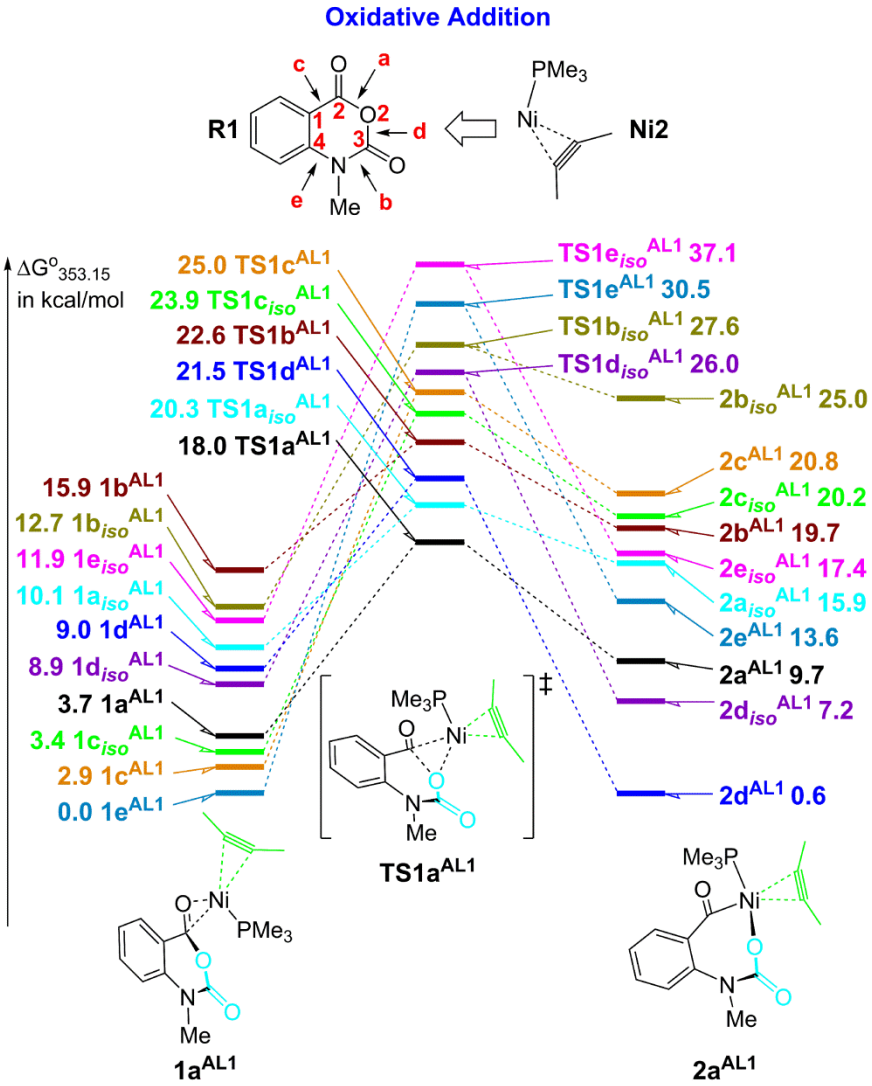

Figure S4. Energy profiles ($\Delta G°_{353.15}$) for the oxidative addition of isatoic anhydride to Ni(PMe_3)(but-2-yne). [a)]The subscript "*iso*" represents that $1x_{iso}^{AL1}$, $TS1x_{iso}^{AL1}$, and $2x_{iso}^{AL1}$ is an isomer of $1x^{AL1}$, $TS1x^{AL1}$, and $2x^{AL1}$ with different position of PMe_3 and alkyne (x = a, b, c, d, and e), respectively.

3. Reaction A Catalyzed by Ni(PMe_3)

We investigated an alternative possibility that the **AL1** participates in the reaction after the decarboxylation process. In this case, a mono-ligated species Ni(PMe_3) (**Ni1**) is an active species. Previous theoretical studies suggested that mono-ligated Ni(0) complex is catalytically more active for [2+2] coupling reaction than the bis-ligated Ni(0) complex.[S15] Hence, it is necessary to investigate the possibility that **Ni1** is an active species and the alkyne participates in the reaction later.

The first step is the oxidative addition of **R1** to **Ni1**. The approach of **R1** to **Ni1** leads to the formation of five kinds of precursor complex, **1a**, **1b**, **1c**, **1d**, and **1e**, where the C2=O1, C3−N, C1=C8, C3=O3 bonds and the benzene ring play a role of coordinating site, as shown in Scheme S3. From these initial precursor complexes, the oxidative addition occurs through similar geometry changes to the corresponding oxidative addition to **Ni2**; see Figure S3. They lead to (a) the C2−O2 bond activation, (b) the C3−N bond activation, (c) the C1−C2 bond activation, and (d) the C3−O2 bond activation, respectively. The benzene η^6-coordination complex **1e** leads to the C4−N bond activation (e). Starting from **1a** and **1d**, the C2−O2 and C3−O2 activations occur in a stepwise manner: in the first step, the Ni center moves from the most stable coordinate site to the target bond, and then the target bond is cleaved by the Ni center. The geometry changes and energy profiles are depicted in Scheme S3 and Figure S5 (a and d paths). The oxidative addition of the C2−O2 bond via the path **1a** → **TS1a** → **2a** → **TS2a** → **3a** is the most favorable among all paths. The $\Delta G^{o\ddagger}$ value going from **1a** to **TS1a** is 14.7 kcal/mol. The C2−O2 distance becomes gradually longer as the reaction proceeds; 1.42 Å (**1a**) → 1.49 Å (**TS1a**) → 1.54 Å (**2a**) → 1.66 Å (**TS2a**) → 2.55 Å (**3a**). In two types of reactions catalyzed by **Ni1** and **Ni2**, it is concluded that the C2−O2 bond is the most reactive for the oxidative addition.

After the oxidative addition, the decarboxylation, the alkyne coordination and insertion, and the reductive elimination occur in this order, as shown in Figure 1(A). The decarboxylation (**3a** → **TS3a** → **4a** → **TS4a** → **5a**) occurs in similar geometric changes to those of reaction **B**. The main difference between these two reactions is that not four-coordinate Ni complex but three-coordinated Ni complex acts as TS and intermediate in reaction **A**. Starting from a three-coordinate d^8 Ni(II) intermediate **5a**, the alkyne coordinates with the Ni center to afford a four-coordinate $\mathbf{4a}^{\mathbf{AL1}}$. After this intermediate, the

elementary step of the reaction **A** is the same as that of the reaction **B**. The last reductive elimination (**7a**^{AL1} → **TS8a**^{AL1} → **10a**^{AL1}) was already described in the main text.

Scheme S3. Schematic representations of five pathways involved in the oxidative addition of isatoic anhydride to Ni(PMe$_3$)

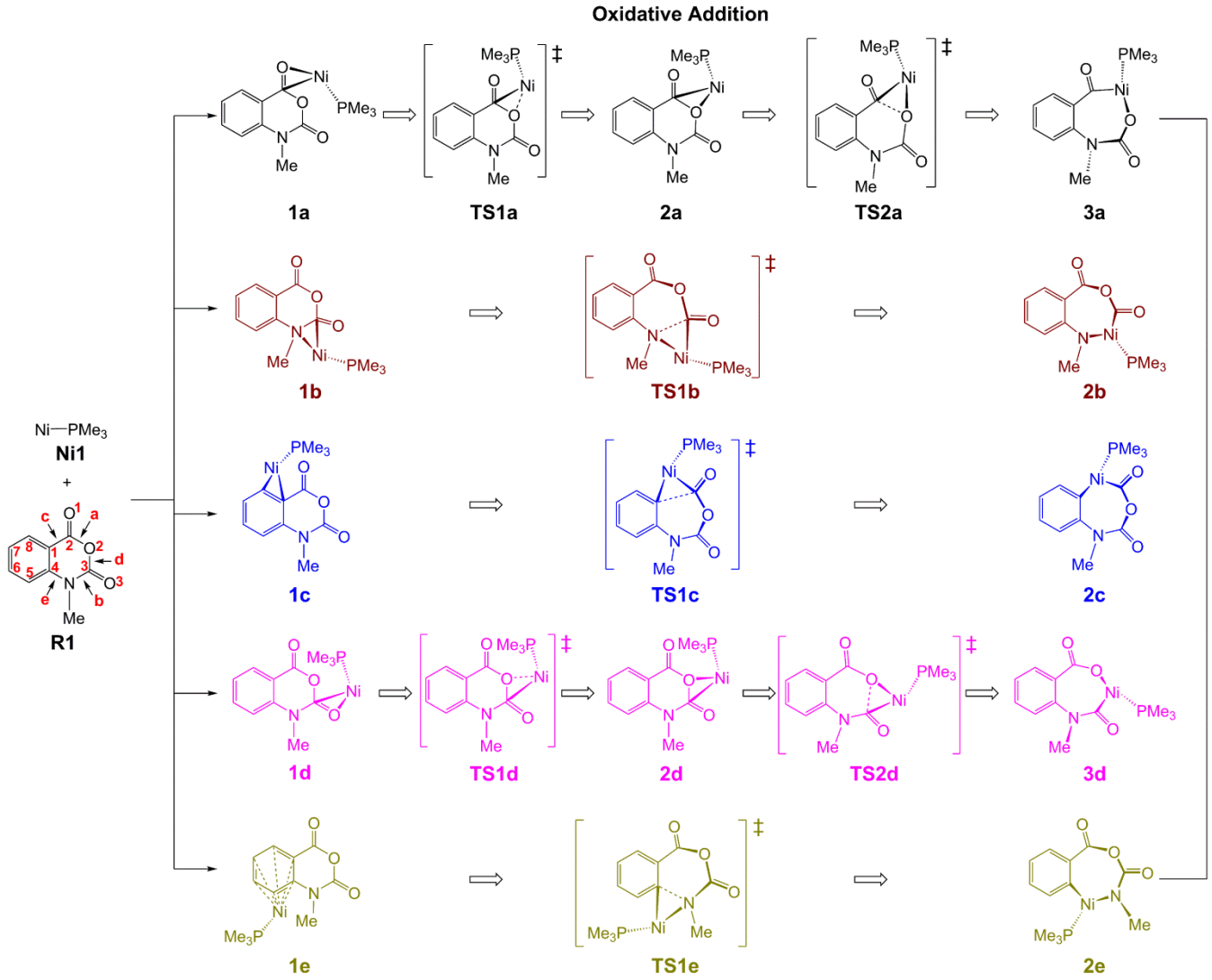

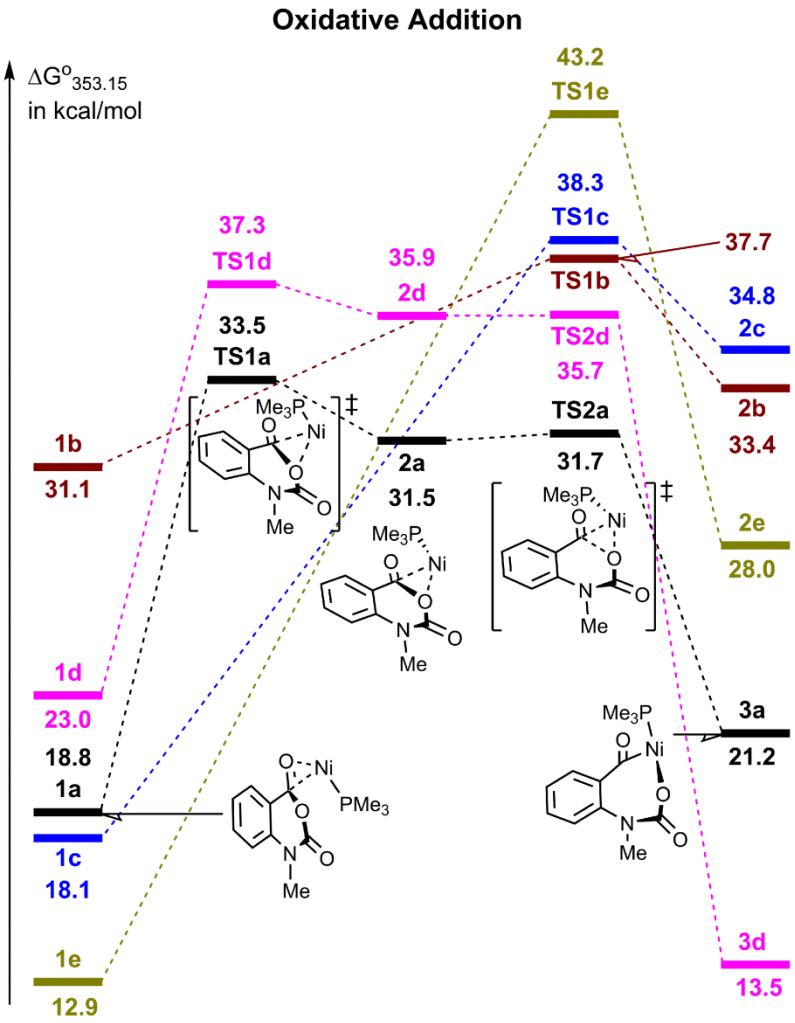

Figure S5. Energy profiles ($\Delta G^{\circ}_{353.15}$) for the oxidative addition of isatoic anhydride to Ni(PMe_3).

4. Fragment MO (FMO) Analysis

Generally, MOs of a total system AB can be represented by a linear combination of MOs of fragments A and B;[22] see eqn (S3):

$$\varphi_i^{AB} = \sum_m C_{im}^A \varphi_m^A + \sum_{mn} C_{in}^B \varphi_n^B \quad \text{(S3)}$$

where φ_i^{AB} represents the *i*th MO of complex AB and φ_m^A and φ_n^B are the *m*th and *n*th MOs of fragments A and B, respectively. C_{im}^A and C_{in}^B are expansion coefficients of φ_m^A and φ_n^B, respectively. Electron populations of φ_m^A and φ_n^B can be obtained from these coefficients.

Table S3. Natural population in the anhydride C2−O2 bond activation

		1a^{AL1}	**TS1a^{AL1}**	**2a^{AL1}**
Ni	s	6.34	6.31	6.35
	p	12.43	12.44	12.42
	d	9.22	9.24	9.15
	total	27.99	27.99	27.93
C2		5.40	5.38	5.48
O2		8.57	8.65	8.70
AL1-1		29.98	29.93	29.87
PMe_3		41.64	41.59	41.51

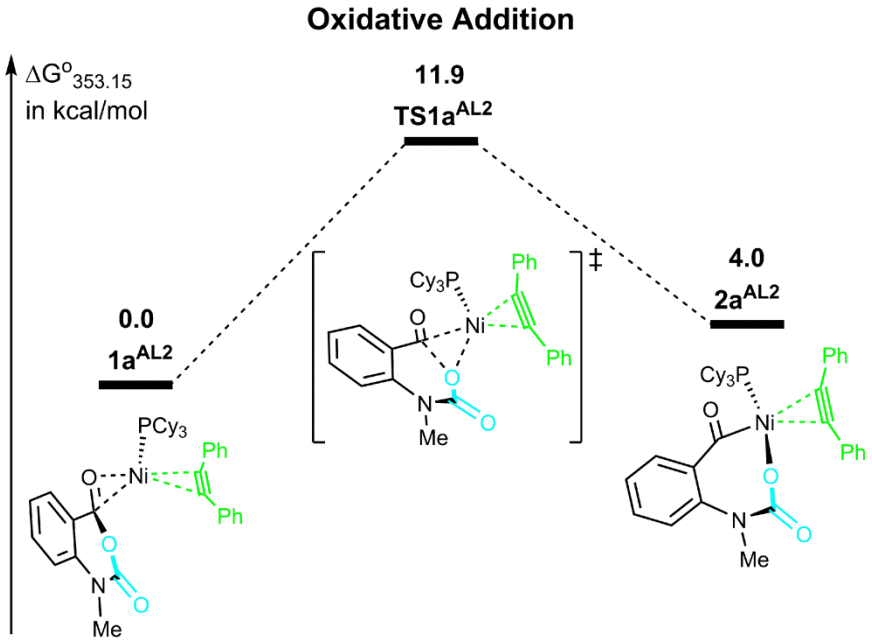

Figure S6. Energy profile ($\Delta G^{o}_{353.15}$) for the C2−O2 bond activation of **R1** to Ni(PCy_3)(AL2).

Table S4. Natural population in the decarboxylation

		2a^{AL1}	**TS2a^{AL1}**	**3a^{AL1}**	**TS3a^{AL1}**	**4a^{AL1}**
Ni	s	6.35	6.35	6.40	6.38	6.44
	p	12.42	12.49	12.43	12.49	12.40
	d	9.15	9.12	9.08	9.10	9.12
	total	27.93	27.97	27.91	27.97	27.96
N		7.53	7.59	7.59	7.64	7.63
CO_2		22.42	22.40	22.36	22.18	
AL1-1		29.87	29.86	29.97	29.89	29.87
PMe_3		41.51	41.49	41.50	41.51	41.55

Scheme S4. Variation of the unoccupied π* orbital energy as a function of the bending angle of AL1

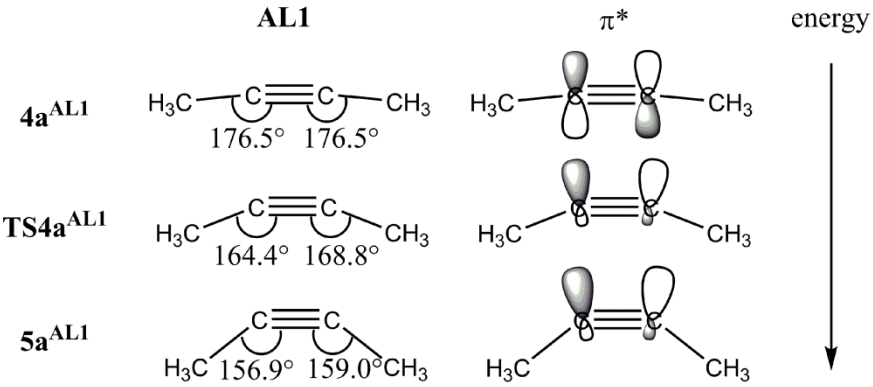

Table S5. Natural population of the alkyne insertion

		4a^{AL1}	**TS4a^{AL1}**	**5a^{AL1}**	**TS5a^{AL1}**	**6a^{AL1}**	**TS5a^{AL1}**	**7a^{AL1}**
Ni	s	6.44	6.37	6.36	6.36	6.37	6.38	6.44
	p	12.40	12.51	12.63	12.56	12.45	12.43	12.29
	d	9.12	9.11	9.08	9.11	9.08	9.08	9.09
	total	27.96	27.99	28.07	28.03	27.90	27.89	27.82
C2		5.49	5.46	5.39	5.41	5.43	5.43	5.42
O1		8.61	8.58	8.53	8.53	8.59	8.60	8.62
N		7.63	7.59	7.59	7.60	7.63	7.64	7.61
C9		6.01	6.06	6.07	6.02	6.04	6.06	6.04
C10		6.01	6.00	6.06	6.11	6.16	6.15	6.16
AL1-1		29.87	29.92	30.03	30.04	30.12	30.13	30.15
PMe_3		41.55	41.60	41.52	41.53	41.46	41.45	41.60

Scheme S5. Kohn-Sham orbital energies of 3d orbitals of Ni^{2+} in the singlet and triplet of 5a^{AL1}

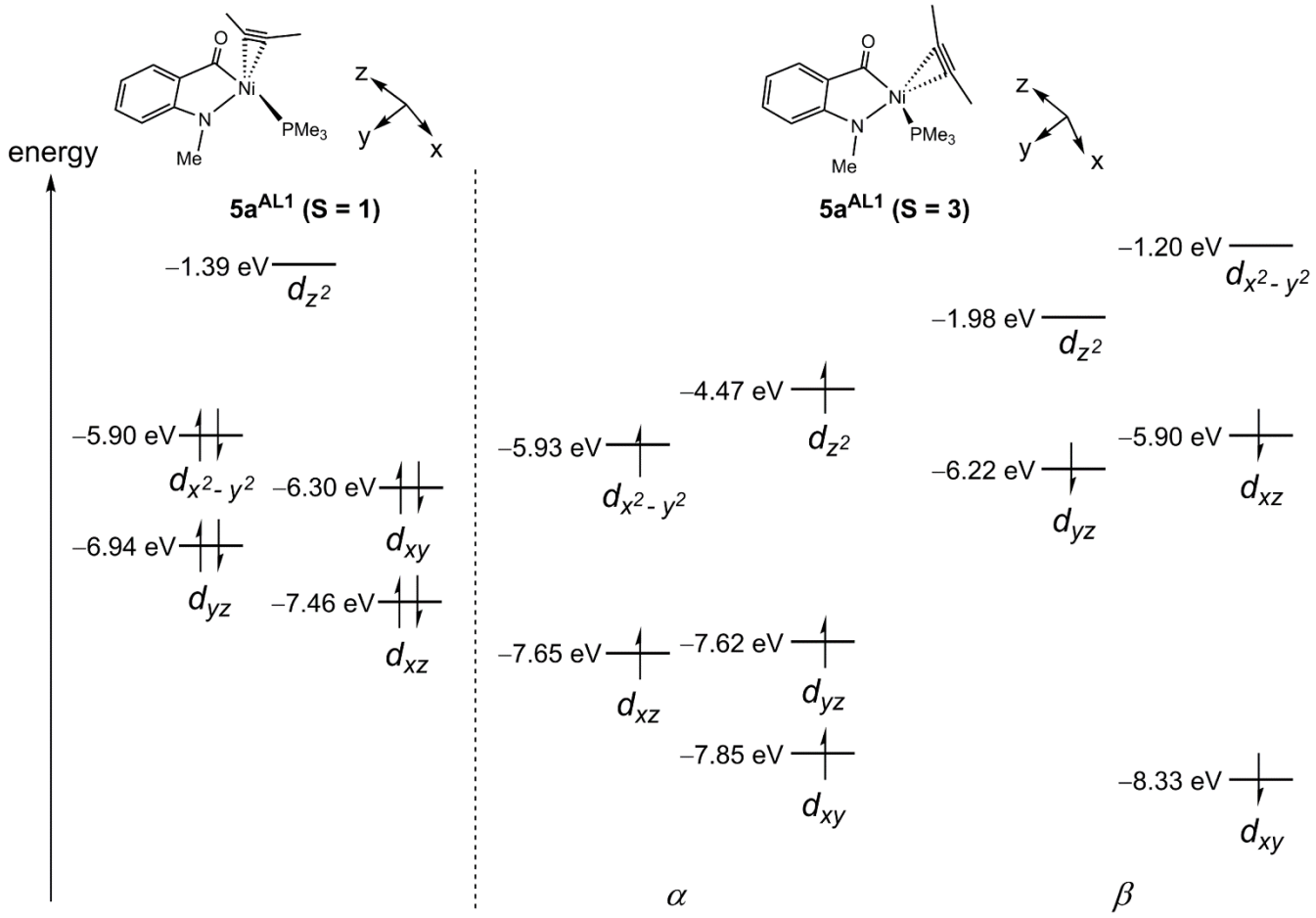

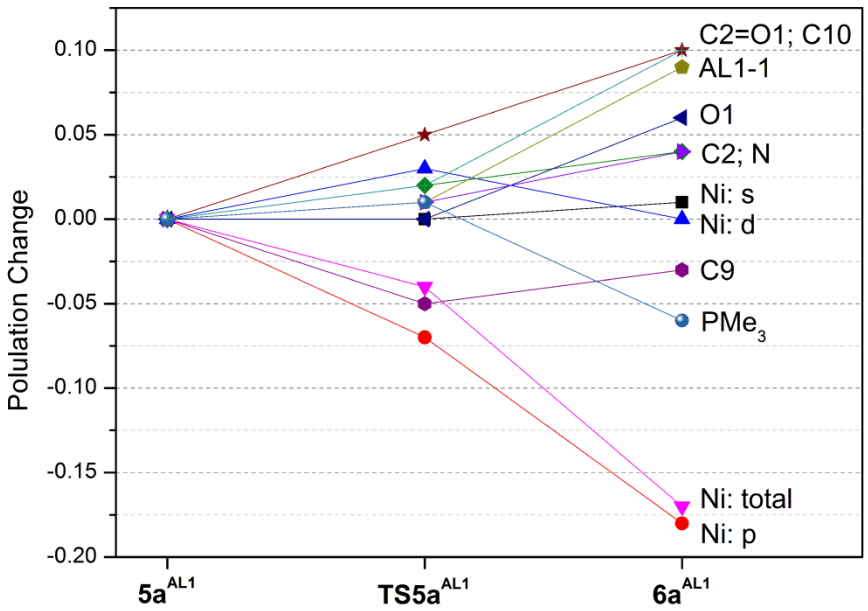

Figure S7. Changes in electron population (in e) in the alkyne insertion.

5. Electronic Process of Reductive Elimination

The reductive elimination is accelerated by the coordination of the second **AL1**, as discussed above. As shown in Table S6 and Figure S8, the N and C9 atomic populations considerably decrease by 0.17 e and 0.24 e, respectively, but the Ni atomic population somewhat increases when going from **8a**$^{\mathbf{AL1}}$ to **9a**$^{\mathbf{AL1}}$. These population changes are consistent with our understanding that this is the reductive elimination. Simultaneously, the electron populations of PMe_3 and the second **AL1** somewhat increase in the reaction. Finally, the second **AL1** becomes negatively charged. These population changes indicate that the electron donations of PMe_3 and alkyne become weaker and the alkyne finally receives electron population from the Ni center to stabilize the Ni(0) species. In other words, alkyne accelerates the reductive elimination by receiving electron population from the Ni center. FMO analyses of **TS7a**$^{\mathbf{AL1}}$ was make here, where **TS7a**$^{\mathbf{AL1}}$ is divided into the dianionic moiety (**P**) and dicationic Ni(PMe_3)(AL1) (**Ni2**) moiety, are shown in Scheme S6. The substantial CT occurs from the σ* anti-bonding orbital (HOMO of **P** moiety) consisting of the p orbitals of the N and C9 atoms (p_N and p_{C9}) to the Ni $3d_\pi$ orbital (LUMO), indicating that the N–C9 bond formation is under progress. Actually, the population on the LUMO of the Ni moiety considerably increases to 1.247 e, while the population on the HOMO of the **P** moiety significantly decreases to 0.726 e. Also, the populations on the HOMO-1 and HOMO-3 of the **P** moiety decrease to 1.898 e and 1.898 e, respectively. Consistent with these decreases, the population on LUMO + 1 of the **Ni2** moiety considerably increases to 0.302 e, where the empty orbital mainly consists of 4p and 3d orbitals of the Ni center. These results clearly indicate that the CT occurs from the p_N and p_{C9} orbitals to the LUMO and LUMO + 1 of the **Ni2** moiety. These CTs contribute to the change of the Ni(II) to the Ni(0) and the formation of a new N−C9 bond.

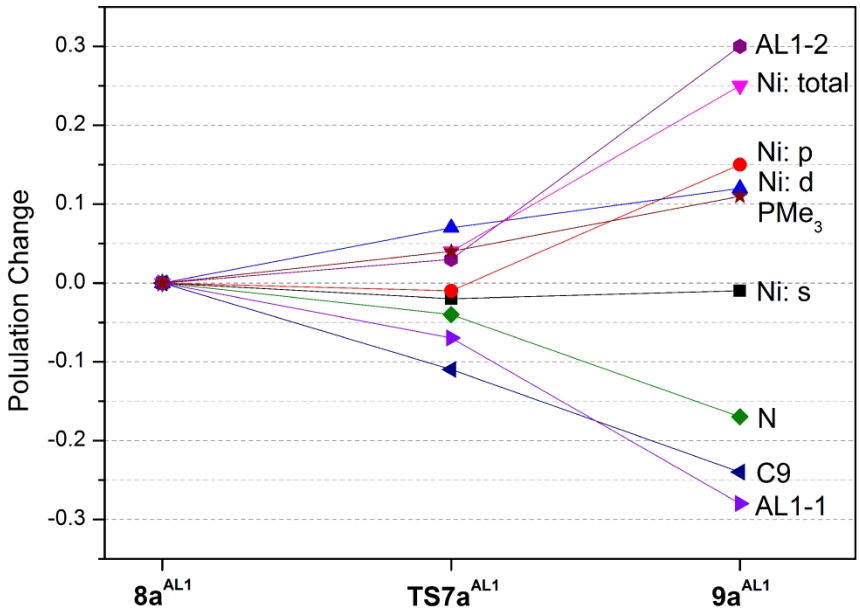

Figure S8. Changes in electron population (in e) in the reductive elimination.

Table S6. Natural population of the reductive elimination

		7a^{AL1}	**8a^{AL1}**	**TS7a^{AL1}**	**9a^{AL1}**
Ni	s	6.44	6.35	6.33	6.34
	p	12.28	12.40	12.39	12.55
	d	9.09	9.12	9.19	9.24
	total	27.81	27.87	27.91	28.12
N		7.61	7.58	7.54	7.41
C9		6.04	6.05	5.94	5.81
AL1-1		30.15	30.18	30.11	29.90
AL1-2			29.86	29.89	30.16
PMe_3		41.61	41.54	41.58	41.65

Scheme S6. Important Kohn-Sham MOs and their electron populations of P moiety and Ni2 moiety in TS7a^{AL1}

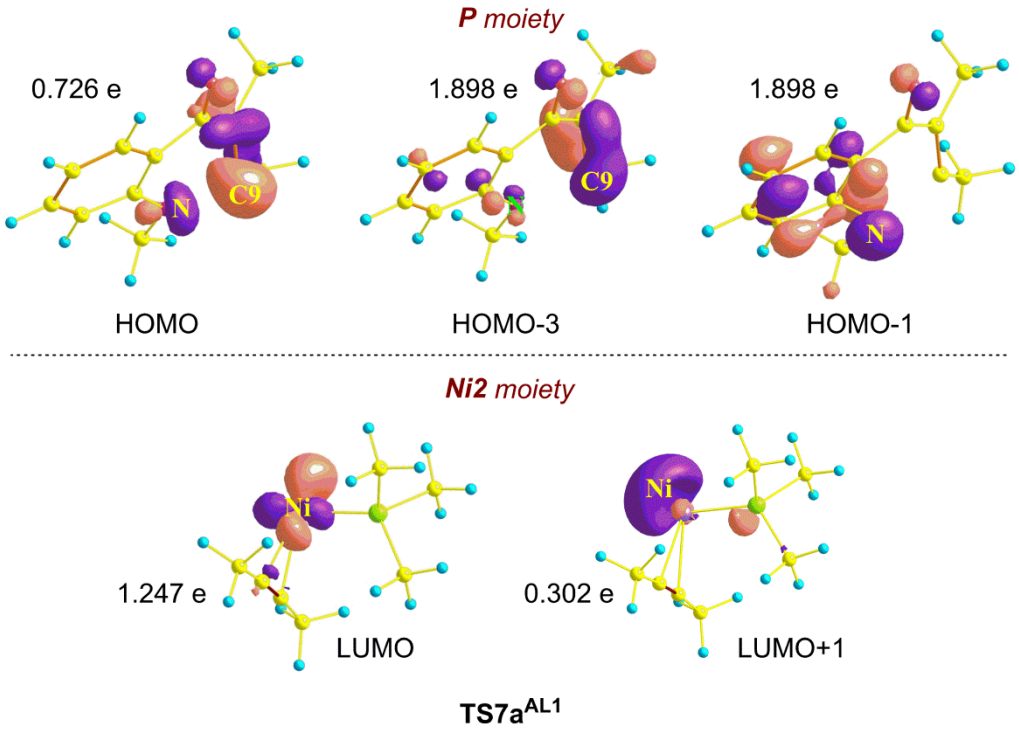

Scheme S7. Schematic representations of structures and LUMOs of R1 and R2

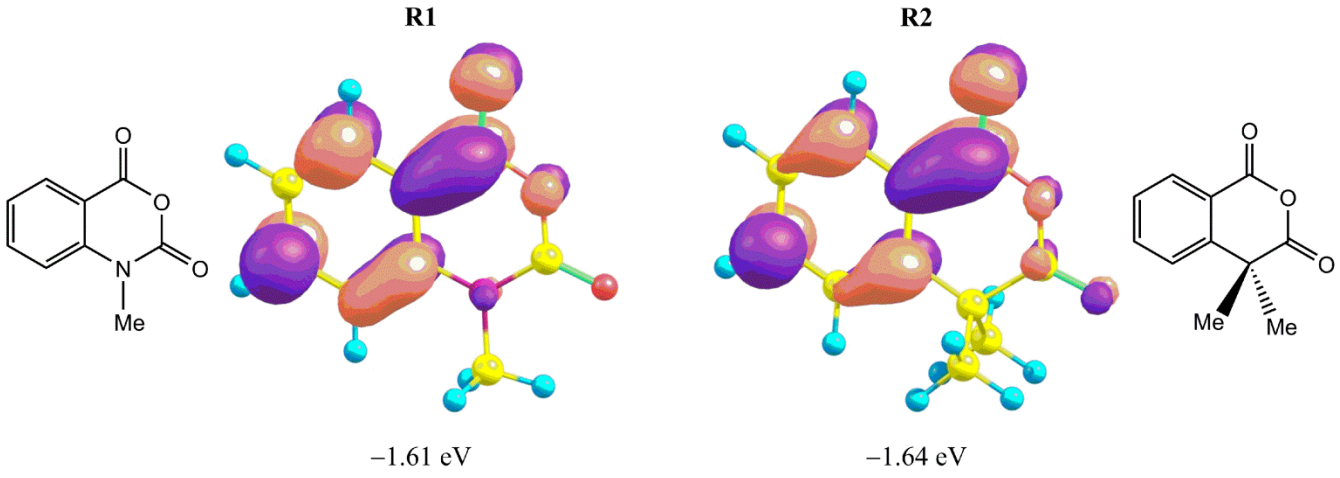

Scheme S8. Electron populations and the HOMO-LUMO features of AL1, AL3, AL4, and AL5

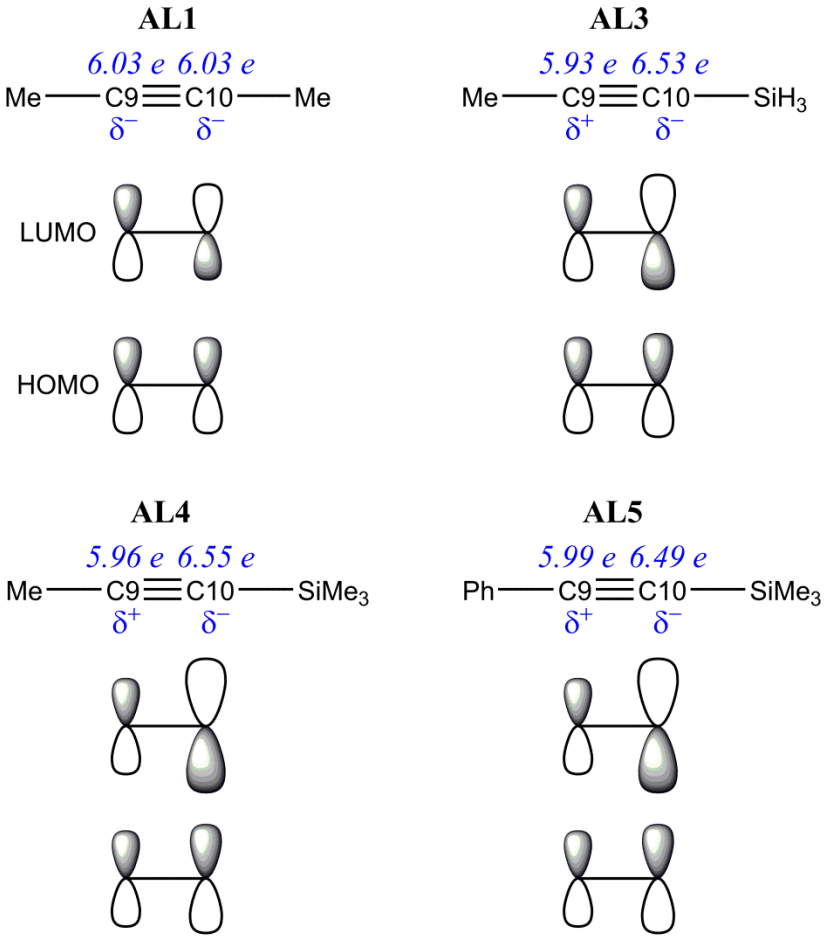

References

S1. (a) Becke, A. D. *Phys. Rev. A* **1988**, *38*, 3098. (b) Becke, A. D. *J. Chem. Phys.* **1993**, *98*, 5648. (c) Perdew, J. P.; Wang, Y. *Phys. Rev. B* **1992**, *45*, 13244.

S2. Grimme, S. *J. Chem. Phys.* **2003**, *118*, 9095.

S3. (a) Head-Gordon, M.; Pople, J. A.; Frisch, M. J. *Chem. Phys. Lett.* **1988**, *153*, 503. (b) Saebø, S.; Almlöf, J. *Chem. Phys. Lett.* **1989**, *154*, 83. (c) Frisch, M. J.; Head-Gordon, M.; Pople, J. A. *Chem. Phys. Lett.* **1990**, *166*, 275. (d) Frisch, M. J.; Head-Gordon, M.; Pople, J. A. *Chem. Phys. Lett.* **1990**, *166*, 281. (e) Head-Gordon, M.; Head-Gordon, T. *Chem. Phys. Lett.* **1994**, *220*, 122.

S4. Zhao, Y.; Truhlar, D. G. *J. Chem. Phys.* **2006**, *125*, 194101.

S5. Zhao, Y.; Truhlar, D. G. *Theor. Chem. Acc.* **2008**, *120*, 215.

S6. (a) Perdew, J. P.; Burke, K; Ernzerhof, M. *Phys. Rev. Lett.* **1996**, *77*, 3865. (b) Perdew, J. P.; Burke, K; Ernzerhof, M. *Phys. Rev. Lett.* **1997**, *78*, 1396. (c) Adamo, C.; Barone, V. *J. Chem. Phys.* **1999**, *110*, 6158.

S7. Grimme, S. *J. Comp. Chem.* **2006**, *27*, 1787.

S8. Chai, J.-D.; Head-Gordon, M. *Phys. Chem. Chem. Phys.* **2008**, *10*, 6615.

S9. Tao, J. M.; Perdew, J. P.; Staroverov, V. N.; Scuseria, G. E. *Phys. Rev. Lett.* **2003**, *91*, 146401.

S10. (a) Krishnan, R.; Binkley, J. S.; Seeger, R.; Pople, J. A. *J. Chem. Phys.* **1980**, *72*, 650. (b) McLean, A. D.; Chandler, G. S. *J. Chem. Phys.* **1980**, *72*, 5639.

S11. (a) Cížek, J. In Advances in Chemical Physics; Hariharan, P. C., Ed.;. Wiley Interscience: New York, 1969; Vol. 14, p 35. (b) Purvis III, G. D.; Bartlett, R. J. *J. Chem. Phys.* **1982**, *76*, 1910. (c) Scuseria, G. E.; Janssen, C. L.; Schaefer III, H. F. *J. Chem. Phys.* **1988**, *89*, 7382. (d) Scuseria, G. E.; Schaefer III, H. F. *J. Chem. Phys.* **1989**, *90*, 3700.

S12. Raghavachari, K.; Pople, J. A. *Int. J. Quantum Chem.* 1978, 14, 91.

S13. (a) Pople, J. A.; Binkley, J. S.; Seeger, R. *Int. J. Quantum Chem. Suppl.* **1976**, *Y-10*, 1. (b) Pople, J. A.; Seeger, R.; Krishnan, R. *Int. J. Quantum Chem. Suppl.* **1977**, *Y-11*, 149.

S14. (a) Sakaki, S.; Ohnishi, Y.; Sato, H. *The Chemical Record* **2010**, *10*, 29. (b) Ishikawa, A.; Nakao, Y.; Sato, H.; Sakaki, S. *Dalton Trans.* **2010**, *39*, 3279. (c) Ishikawa, A.; Nakao, Y.; Sato, H.; Sakaki, S. *Inorg. Chem.* **2009**, *48*, 8154. (d) Ohnishi, Y.; Nakao, Y.; Sato, H.; Hiyama, T.; Sakaki, S. *Organometallics* **2009**, *28*, 2583.

S15. (a) Li, Z.; Zhang, S.-L.; Fu, Y.; Guo, Q.-X.; Liu, L. *J. Am. Chem. Soc.* **2009**, *131*, 8815. (b) Quasdorf, K. W.; Antoft-Finch, A.; Liu, P.; Silberstein, A. L.; Komaromi, A.; Blackburn, T.; Ramgren, S. D.; Houk, K. N.; Snieckus, V.; Garg, N. K. *J. Am. Chem. Soc.* **2011**, *133*, 6352.

Complete Representation of Ref. 19.

Frisch, M. J.; Trucks, G. W.; Schlegel, H. B.; Scuseria, G. E.; Robb, M. A.; Cheeseman, J. R.; Scalmani, G.; Barone, V.; Mennucci, B.; Petersson, G. A.; Nakatsuji, H.; Caricato, M.; Li, X.; Hratchian, H. P.; Izmaylov, A. F.; Bloino, J.; Zheng, G.; Sonnenberg, J. L.; Hada, M.; Ehara, M.; Toyota, K.; Fukuda, R.; Hasegawa, J.; Ishida, M.; Nakajima, T.; Honda, Y.; Kitao, O.; Nakai, H.; Vreven, T.; Montgomery, Jr., J. A.; Peralta, J. E.; Ogliaro, F.; Bearpark, M.; Heyd, J. J.; Brothers, E.; Kudin, K. N.; Staroverov, V. N.; Kobayashi, R.; Normand, J.; Raghavachari, K.; Rendell, A.; Burant, J. C.; Iyengar, S. S.; Tomasi, J.; Cossi, M.; Rega, N.; Millam, J. M.; Klene, M.; Knox, J. E.; Cross, J. B.; Bakken, V.; Adamo, C.; Jaramillo, J.; Gomperts, R.; Stratmann, R. E.; Yazyev, O.; Austin, A. J.; Cammi, R.; Pomelli, C.; Ochterski, J. W.; Martin, R. L.; Morokuma, K.; Zakrzewski, V. G.; Voth, G. A.; Salvador, P.; Dannenberg, J. J.; Dapprich, S.; Daniels, A. D.; Farkas, Ö.; Foresman, J. B.; Ortiz, J. V.; Cioslowski, J.; Fox, D. J. Gaussian 09, Revision B.01, Gaussian, Inc., Wallingford, CT, 2010.